Isentropic Slopes, Downgradient Eddy Fluxes, and the Extratropical Atmospheric Circulation Response to Tropical Tropospheric Heating

AMY H. BUTLER

NOAA/NWS/NCEP/Climate Prediction Center, Camp Springs, Maryland

DAVID W. J. THOMPSON AND THOMAS BIRNER

Department of Atmospheric Science, Colorado State University, Fort Collins, Colorado

(Manuscript received 13 December 2010, in final form 17 May 2011)

ABSTRACT

Climate change experiments run on Intergovernmental Panel on Climate Change (IPCC)–class numerical models consistently suggest that increasing concentrations of greenhouse gases will lead to a poleward shift of the midlatitude jets and their associated eddy fluxes of heat and potential vorticity (PV). Experiments run on idealized models suggest that the poleward contraction of the jets can be traced to the effects of increased latent heating and thus locally enhanced warming in the tropical troposphere. Here the authors provide new insights into the dynamics of the circulation response to tropical tropospheric heating using transient experiments in an idealized general circulation model.

It is argued that the response of the midlatitude jets to tropical heating is driven fundamentally by 1) the projection of the heating onto the meridional slope of the lower tropospheric isentropic surfaces, and 2) a diffusive model of the eddy fluxes of heat and PV. In the lower and middle troposphere, regions where the meridional slope of the isentropes (i.e., the baroclinicity) is increased are marked by anomalously poleward eddy fluxes of heat, and vice versa. Near the tropopause, regions where the meridional gradients in PV are increased are characterized by anomalously equatorward eddy fluxes of PV, and vice versa. The barotropic component of the response is shown to be closely approximated by the changes in the lower-level heat fluxes. As such, the changes in the eddy fluxes of momentum near the tropopause appear to be driven primarily by the changes in wave generation in the lower troposphere.

1. Introduction

Anthropogenic emissions of greenhouse gases are linked in a range of numerical experiments to a robust poleward contraction of the midlatitude jets and their associated eddy fluxes of heat and momentum (Fyfe et al. 1999; Kushner et al. 2001; Yin 2005; Miller et al. 2006; Arblaster and Meehl 2006; Hegerl et al. 2007; Lu et al. 2008; Schneider et al. 2010). The poleward shift of the jets projects onto annular modes of climate variability (e.g., Kushner et al. 2001; Miller et al. 2006) and thus has pronounced implications for climate change throughout the extratropics. The simulated response of the midlatitude jets to increasing carbon dioxide is among the most robust circulation responses found in climate change experiments run on fully coupled Intergovernmental Panel on Climate Change (IPCC)–class models (Hegerl et al. 2007).

The amplification of tropospheric warming by increased latent heating in the tropics has been hypothesized to be a key factor in driving the simulated trends in the midlatitude jets. For example, Lim and Simmonds (2008) demonstrate that the latitude of the Southern Hemisphere midlatitude jet is sensitive to tropical heating in their full-physics atmospheric general circulation model, and Butler et al. (2010) demonstrate that the poleward contraction of the midlatitude jets is a robust response to climate change–like heating in the tropical troposphere in an idealized atmospheric general circulation model. Chen and Held (2007) and Lu et al. (2008) point to the importance of changes in the meridional temperature gradient near the tropopause level in driving the shift of the jet in climate change simulations, although they do not explicitly link the shift in the jet to tropical heating.

Corresponding author address: Amy H. Butler, 5200 Auth Road, Camp Springs, MD 20746.
E-mail: amy.butler@noaa.gov

DOI: 10.1175/JAS-D-10-05025.1

The mechanisms whereby tropical heating drives a poleward shift in the midlatitude jets remain unclear. Tropical heating is expected to drive an eastward acceleration of the flow in the midlatitude upper troposphere/lower stratosphere via thermal wind balance. But the response of the thermal wind does not explain the simulated changes in the eddy fluxes of heat and momentum that accompany the poleward shift in the jet. The eddy response has been interpreted in the context of changes in subtropical static stability (Frierson 2008; Lu et al. 2008), changes in the height of the tropopause (Williams 2006; Lorenz and DeWeaver 2007), changes in the surface temperature gradient (Brayshaw et al. 2008; Lu et al. 2010; Chen et al. 2010), changes in the eddy length scale (Kidston et al. 2011), and the influence of the thermally driven eastward wind anomalies on the Rossby wave phase speed (Chen and Held 2007; Chen et al. 2008). In the latter case, the increase in the Rossby wave phase speed leads to a poleward shift in the region of maximum wave breaking in the subtropics, and through the adjustment of the meridional circulation, a poleward shift in the low-level baroclinic zone (e.g., Robinson 2000).

The purpose of this study is to provide an alternative perspective on the response of the midlatitude tropospheric circulation to zonal-mean tropical heating. The response is interpreted in the context of a) the projection of the heating onto the climatological-mean isentropic surfaces and thus the influence of the heating on the meridional slope of the lower tropospheric isentropic surfaces and b) a diffusive model of the eddy fluxes of heat near the surface and potential vorticity (PV) near the tropopause. In the following section we outline the premise for our guiding hypothesis. Section 3 reviews the experiment design and analysis details. Results are given in section 4 and are discussed in section 5.

2. Guiding hypothesis

The role of the eddy fluxes in the atmospheric general circulation can be approached in two ways:

1) Eddies are treated as (Rossby) waves. They are generated near the surface in regions of large baroclinicity, their propagation is determined by the index of refraction, and they dissipate in regions determined by wave properties such as wavenumber and phase speed (e.g., Matsuno 1970; Chen and Robinson 1992).
2) Eddies are treated as (macro) turbulence. They act fundamentally to diffuse heat near the surface in regions of large baroclinicity (e.g., Kushner and Held 1998; Held 1999; Held and Schneider 1999; Schneider 2004) and PV in the free atmosphere in regions of large PV gradients (e.g., Green 1970; Held 1999).

Potential vorticity is intimately tied to both perspectives. Rossby waves owe their existence to basic state PV gradients, and the refractive index is a function of the PV gradient. Eddy turbulence is described by diffusive eddy fluxes of PV and these are often parameterized to be proportional to the basic state PV gradient. But in the wave perspective, the eddy fluxes of heat and PV are determined by waveguides, phase speeds, and other wave properties. In the (macro) turbulence perspective, the eddy fluxes are determined primarily by the eddy diffusivities. Nevertheless, both wave and turbulence perspectives are closely related: breaking Rossby waves lead to turbulent eddy fluxes and these in turn form and maintain waveguides through self-sharpening of basic state PV gradients (e.g., McIntyre 2008).

The diffusive model provides an excellent approximation of the eddy fluxes of heat near the surface where radiation plays a dominant role in setting the mean temperature gradients (e.g., Kushner and Held 1998; Held 1999). The interpretation of the diffusive model is more nuanced in the free atmosphere where the eddies play a more prominent role in determining the mean gradients in PV (Held 1999; see also our section 5b). Nevertheless, as demonstrated here, the diffusive model of the PV fluxes provides a seemingly robust qualitative estimate for the changes in the eddy fluxes of PV driven by diabatic heating.

The guiding hypotheses of our analysis are as follows:

a) Diabatic heating in the tropical troposphere has two direct effects on the extratropical circulation: 1) the heating adjusts the meridional slope of the isentropes in the free troposphere and 2) the heating adjusts the distribution of PV at the tropopause via its influence on atmospheric static stability (i.e., the thickness of the isentropic layers).
b) The eddy fluxes of heat and PV adjust to the direct effects of the heating in a manner consistent with the flux–gradient relationship. At lower levels, the poleward eddy fluxes of heat are increased in regions where the isentropic slopes are anomalously steep (i.e., the baroclinicity is increased) and decreased where the isentropic slopes are flattened. At upper levels, the equatorward eddy fluxes of PV are increased where the pole–equator gradients in PV are enhanced and decreased where the gradients are diminished. Note that in the diffusive model the eddy fluxes are a function of not only the mean gradients but also the eddy diffusivities. As discussed in section 5, our approach implicitly assumes that the diffusivities remain largely unchanged in response to the heating.

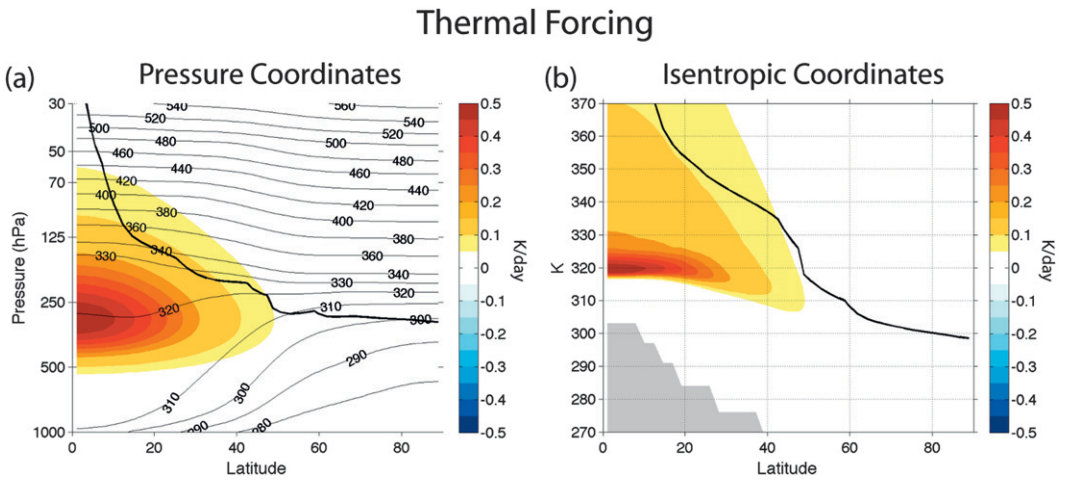

FIG. 1. (a) The time-mean, ensemble-mean potential temperature for the unforced experiment (contours) and the applied thermal forcing (shading) in pressure coordinates. Note that the contour interval changes from tropospheric to stratospheric levels. (b) The applied thermal forcing in isentropic coordinates. The gray shading indicates regions where the isentropes intersect the surface. Units are K day^{-1} for the forcing and K for the isentropic surfaces. The solid black line represents the height of the dynamic tropopause, defined as the contour where PV = 2 PVU.

In the following section we outline the experiment design and provide details of the analyses. Results are presented in section 4.

3. Experiment design and analysis details

a. Experiment design

We test the above hypotheses by examining the transient response to tropical heating in the dry dynamical core of the Colorado State University general circulation model (Ringler et al. 2000). The model is identical to that used in Butler et al. (2010). The vertical coordinate system is hybrid sigma–isentropic (Konor and Arakawa 1997) and transitions from sigma near the surface to isentropic in the free troposphere and stratosphere. There is no topography, no ocean, and there are 25 vertical layers with a model top at 1 hPa. The model is discretized on a geodesic grid (Heikes and Randall 1995) with 10 242 grid cells (a horizontal resolution of about 250 km).

All experiments are run with Held–Suarez (Held and Suarez 1994) parameterizations, and the circulation is driven by Newtonian relaxation toward an equinoctial radiative equilibrium temperature profile. The impact of using a wintertime radiative equilibrium profile was tested in Butler et al. (2010) and found to have only a small qualitative effect on the atmospheric response to tropical tropospheric heating.

The heating is given in Butler et al. (2010; cf. their Fig. 2a and Table 1) and is reproduced here in Fig. 1. The forcing is zonally symmetric, has peak amplitude of 0.5 K day^{-1}, and is centered at about 300 hPa and the equator. Changes in the depth, altitude, and shape of the tropical thermal forcing affect the amplitude of the extratropical response (Butler et al. 2010; cf. their Fig. 2). But as discussed further in section 5 (and demonstrated in Butler et al. 2010), the poleward shift of the middle latitude jet is reproducible when the heating is contracted in the vertical and meridional directions. The weak projection of the heating in the lower tropical stratosphere does not affect the results in a notable manner (Butler et al. 2010; cf. their Fig. 2).

Since we will be examining the response in terms of the isentropic slope and the eddy flux of PV on isentropic surfaces, the heating is superposed on the model isentropes in Fig. 1a and is transposed into an isentropic coordinate system in Fig. 1b. Note that the isentropic surfaces in the lower midtroposphere tilt upward with latitude (Fig. 1a). Thus, for the thermal forcing considered here, the isentropes below about 320 K experience peak heating not at the equator but at subtropical latitudes (Fig. 1b). The solid black lines in Figs. 1a and 1b denote the dynamical tropopause, defined here as the level at which PV is equal to 2 PV units (1 PVU = 10^{-6} m^2 s^{-1} K kg^{-1}).

The steady-state response to the heating was explored in Butler et al. (2010). Here we consider the transient response. The transient simulations are started from 12 different initial conditions generated from a control run that has been spun up for 360 days. The initial conditions are separated by 50 days to ensure independence. In the forced experiments, the thermal forcing is turned on after 10 days, and each member run lasts 150 days. In the unforced experiments, the thermal forcing remains off at all time steps. The use of an equinoctial equilibrium temperature profile provides twice the sample size assuming the responses in the two hemispheres are independent of

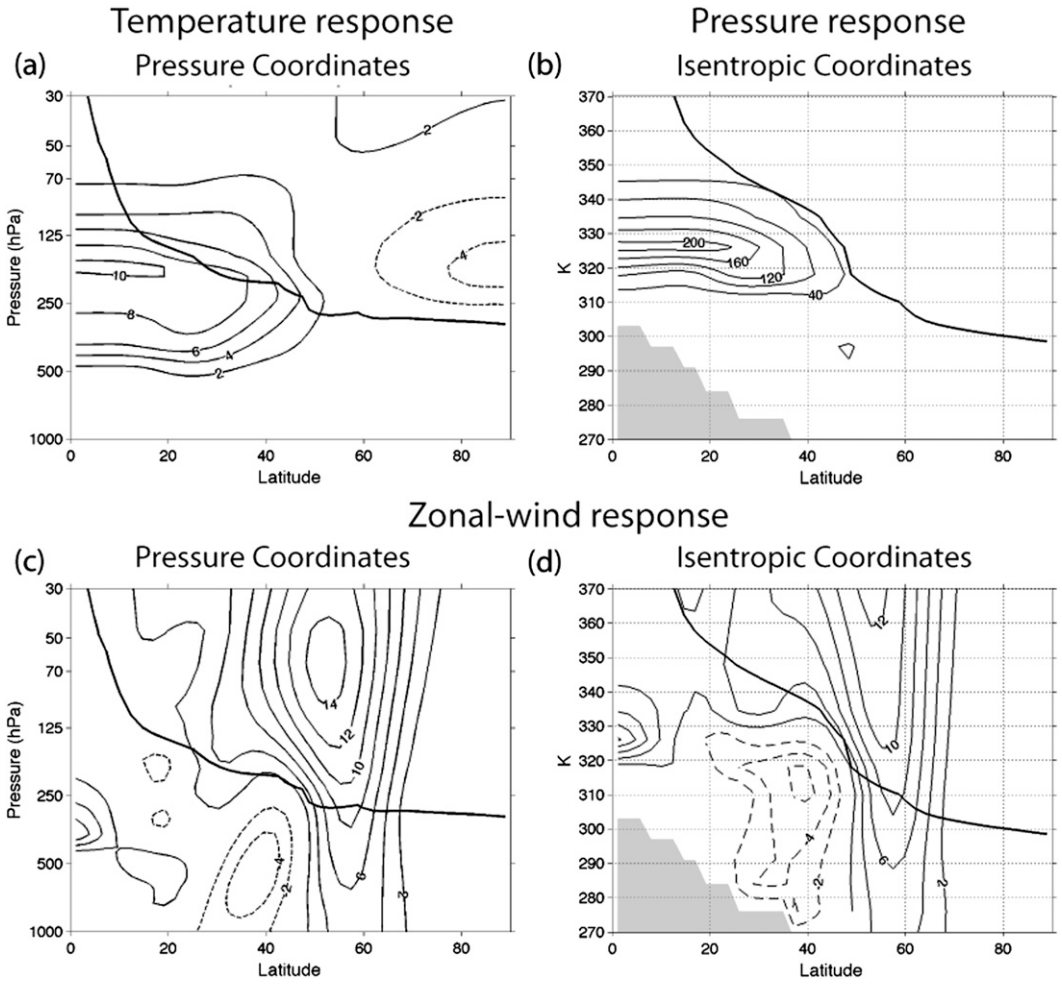

FIG. 2. (a) The temperature response to the thermal forcing. Contour interval is 2 K. (b) The pressure response in isentropic coordinates. Contour interval is 40 hPa. (c) The response of the zonal wind to the thermal forcing. Contour interval is 2 m s^{-1}. (d) As in (c), but for isentropic coordinates. In all panels, the response is defined as the difference between the ensemble mean of the forced experiment and the ensemble mean of the unforced experiment. The response is averaged over days 100–150. The solid black line indicates the contour where PV = 2 PVU. The zero line is omitted.

each other. Thus, there are 24 ensemble members in the forced and unforced experiments.

In all figures, the ''response'' is defined as the difference between the ensemble mean of the 24 forced runs and the ensemble mean of the 24 unforced runs. The statistical significance of key aspects of the steady-state response is established in Butler et al. 2010 (see their Tables 2 and 4). All key results highlighted here (i.e., changes in the zonal wind, PV, isentropic slope, and the eddy fluxes of heat and PV) are qualitatively reproducible in all 24 ensemble members.

b. *Analysis details*

The response to the thermal forcing is examined in the context of the isentropic slope and the eddy fluxes of heat and PV. The eddy fluxes of heat are examined on pressure levels in the lower troposphere since isentropic surfaces intersect the surface. Potential vorticity and the eddy fluxes of PV are examined on isentropic surfaces at and above 300 K. Potential vorticity is defined on isentropic surfaces as

$$P = \frac{(f + \zeta)}{\sigma}, \tag{1}$$

where the isentropic density (the inverse of the ''thickness'' of the isentropic layer) is

$$\sigma = -\frac{1}{g} \cdot \frac{\partial p}{\partial \theta}. \tag{2}$$

In (1) and (2), P is the potential vorticity, f is the planetary vorticity, ζ is the relative vorticity calculated on isentropic surfaces, g is the gravitational constant, θ is potential temperature, and p is pressure.

The eddy fluxes of PV in isentropic coordinates are mass weighted and are calculated in the following manner. First, the mass-weighted zonal-mean meridional wind v and P are found as

$$\overline{v}^* = \frac{\overline{\sigma v}}{\overline{\sigma}} \quad \text{and} \quad \overline{P}^* = \frac{\overline{\sigma P}}{\overline{\sigma}}, \tag{3}$$

where the overbars denote the zonal mean and the asterisks denote mass-weighted zonal-mean quantities. The eddy components of the mass-weighted meridional wind and potential vorticity fields are subsequently found as

$$\hat{v} = v - \overline{v}^* \quad \text{and} \quad \hat{P} = P - \overline{P}^*, \tag{4}$$

where hats denote deviations from the mass-weighted zonal mean. Finally, the mass-weighted zonal-mean eddy fluxes of PV (10^{-6} m^3 s^{-2} K kg^{-1} or, equivalently, PVU m s^{-1}) are calculated as

$$\overline{\hat{v}\hat{P}}^* = \frac{\overline{\sigma \hat{v} \hat{P}}}{\overline{\sigma}}. \tag{5}$$

In isentropic coordinates, the eddy PV flux is directly related to the convergence of the Eliassen–Palm (EP) flux—and thus to the eddy fluxes of thickness (i.e., heat) and momentum—as

$$\begin{aligned} \frac{\overline{\sigma \hat{v} \hat{P}}}{\overline{\sigma}} &\cong \frac{1}{\overline{\sigma}} \nabla \cdot \mathbf{F} \\ &\cong \frac{1}{\overline{\sigma}} \cdot \left[-\overline{v' \frac{\partial}{a \partial \varphi} u'} - \frac{1}{\overline{\sigma}} \left(f - \frac{\partial}{a \partial \varphi} \overline{u} \right) \overline{\sigma' v'} \right], \end{aligned} \tag{6}$$

where $\nabla \cdot \mathbf{F}$ is the divergence of the EP flux vector, u is the zonal wind, a is the radius of the earth, and φ is latitude [e.g., Tung 1986, (4.3)]. The first term on the right-hand side (rhs) corresponds to the meridional divergence of the eddy flux of zonal momentum. The second term on the rhs corresponds to the vertical divergence of the eddy flux of heat. Recall that in isentropic coordinates, the eddy fluxes of heat correspond to fluxes of thickness and are thus analogous to form drag.

4. Results

Figure 2 shows the response of (top) zonal-mean temperature and (bottom) zonal wind to the heating averaged over days 100–150 of the integration. The results are shown in (left) pressure and (right) isentropic coordinates. Note that the temperature response is converted to pressure when shown in isentropic coordinates (i.e., warming corresponds to the movement of isentropic surfaces to higher pressures). The temperature response (top) includes warming that spans the entire tropics and cooling in the lower polar stratosphere. The polar stratospheric cooling results from anomalous weakening of the stratospheric residual circulation (Butler et al. 2010) and is not examined here. Note that because of the meridional slope of the mean isentropic surfaces, the pressure response below about 320 K is largest not at the equator but at subtropical latitudes (Fig. 2b).

Figure 3 highlights the time-varying response to the heating in the zonal wind at (top) 350 K and (bottom) 700 hPa. The response in the upper troposphere/lower stratosphere (e.g., ~350 K) is eastward throughout the middle latitudes (Figs. 2d and 3a). In contrast, the response in the lower troposphere (e.g., ~700 hPa) is characterized by a dipole in the zonal wind field, with eastward anomalies located between about 50° and 70° and westward anomalies between about 30° and 40° (Figs. 2c and 3b). Interestingly, the changes in the near-surface wind field propagate poleward by about 5° throughout the 150 days of the transient integration (Fig. 3b). The response is near equilibrium by about day 100 of the integration (Fig. 3) and thus the response averaged over days 100–150 bears a strong resemblance to the steady-state response to the same heating [i.e., compare Figs. 2a and 2c from this study with Fig. 2a from Butler et al. (2010)].

As demonstrated in Butler et al. (2010), the response to the heating is consistent with a poleward shift in the model midlatitude tropospheric jet. The dipole in the tropospheric wind field reflects a poleward shift in the latitude of maximum surface westerlies and is accompanied by three statistically significant changes in the eddy fluxes (Butler et al. 2010; cf. their Fig. 2a): 1) anomalously poleward eddy fluxes of zonal momentum in the upper troposphere across about 50°, 2) anomalously poleward eddy heat fluxes in the lower troposphere poleward of about 40°, and 3) anomalously equatorward eddy heat fluxes in the lower troposphere equatorward of about 40°. Below we first consider the response in terms of the eddy fluxes of heat in the free troposphere. We then consider the response of the eddy fluxes of PV at the tropopause. The barotropic component of the response (i.e., the component driven by the eddy fluxes of momentum) is considered in the discussion section.

a. Eddy fluxes of heat in the troposphere

In a baroclinic atmosphere, the climatological-mean pressure and isentropic surfaces are not parallel. Thus, a heating profile that varies monotonically along pressure surfaces will, in general, not vary monotonically along isentropic surfaces. The projection of the heating onto the climatological-mean isentropic surfaces is important, as

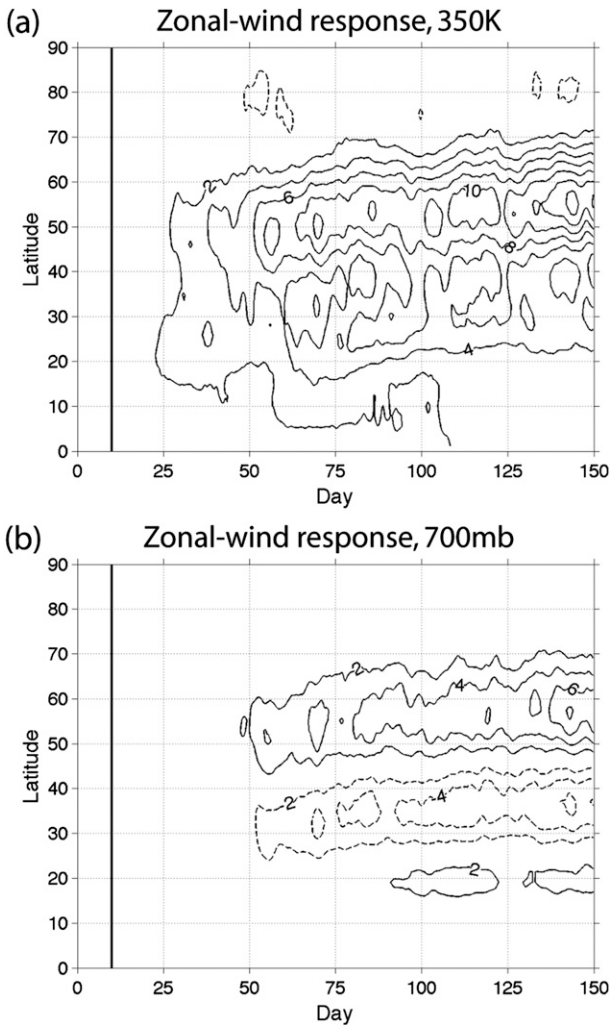

FIG. 3. The response of the zonal wind as a function of time and latitude at (a) 350 K and (b) 700 hPa. The heating is turned on at day 10 (solid vertical line). Contour interval is 2 m s^{-1}. The zero line is omitted.

the projection determines the effect of the heating on the meridional slope of the isentropic surfaces. The meridional slope of the isentropic surfaces in turn plays a key role in the development of baroclinic waves: it is equivalent to the baroclinicity of the flow and is implicitly included in metrics of instability such as Eady growth rate (i.e., the Eady growth rate is proportional to the ratio of the meridional gradient and square root of the vertical gradient in temperature; Lindzen and Farrell 1980).

The initial response of the meridional slope of the isentropes when the tropical heating is turned on can be expressed analytically as follows. First, define the meridional slopes of the isentropic surfaces as

$$s_\theta = -\frac{\partial\theta/\partial y}{\partial\theta/\partial z}, \tag{7}$$

where θ denotes the potential temperature. Similarly, define the meridional slope of the tropical heating as

$$s_{\tilde{Q}} = -\frac{\partial\tilde{Q}/\partial y}{\partial\tilde{Q}/\partial z}, \tag{8}$$

where $\tilde{Q}$ denotes the tropical heating in units of $\partial\theta/\partial t$. The time rate of change of the meridional slope of the isentropic surfaces when the heating is turned on is given by the derivative of (7) with respect to time:

$$\frac{\partial s_\theta}{\partial t} \cong -\frac{\partial\tilde{Q}/\partial y}{\partial\theta/\partial z} - s_\theta\frac{\partial\tilde{Q}/\partial z}{\partial\theta/\partial z} = (s_{\tilde{Q}} - s_\theta)\frac{\partial\tilde{Q}/\partial z}{\partial\theta/\partial z}, \tag{9}$$

where we have assumed that when the heating is initially turned on, $\partial\theta/\partial t \cong \tilde{Q}$.

Equation (9) makes clear that the initial rate of change of the isentropic slopes is a function of the meridional and vertical structure of both the heating (i.e., the thermal forcing) and the isentropic surfaces. If the meridional slope of the heating $s_{\tilde{Q}}$ is less than s_θ, then s_θ will decrease where the heating grows with height ($\partial\tilde{Q}/\partial z > 0$) and increase where the heating damps with height ($\partial\tilde{Q}/\partial z < 0$). Equation (9) also makes clear that the heating will always change the isentropic slope except where (i) the slopes of the heating and the isentropes are identical (i.e., if $s_{\tilde{Q}} - s_\theta = 0$) or (ii) the vertical gradient of the heating is zero. These conditions are possible locally but not globally unless (i) the heating extends from pole to pole or (ii) the heating is uniform with height.

In the case of the tropical heating considered here, $\tilde{Q}$ decreases uniformly with latitude on pressure surfaces (Fig. 1a). Since the climatological-mean isentropic surfaces below about 320-K slope upward with latitude (Fig. 1a, solid contours), it follows that such isentropes will experience the largest heating (and hence largest pressure rises) not at the equator but in the subtropics (Figs. 1b and 2b). Thus, the isentropic slope will be reduced in the subtropics and increased at middle latitudes. In the context of (9), $\partial\tilde{Q}/\partial z > 0$ and $s_{\tilde{Q}} - s_\theta < 0$ below the level of maximum heating in the subtropics, whereas $\partial\tilde{Q}/\partial z > 0$ and $s_{\tilde{Q}} - s_\theta > 0$ below the level of maximum heating in middle latitudes.

For example, consider the response of the isentropic slope at 310 K. Figure 4a shows the projection of the thermal forcing on the 310-K surface (contours) and the response in pressure on the 310-K surface (shading) as a function of time and latitude. The thermal forcing projects most strongly onto the 310-K isentropic surface not at the equator but around 40°–50° (Fig. 4a, contours; see also Fig. 2b). As the 310-K surface is heated, it moves to higher pressure in approximately the same latitude

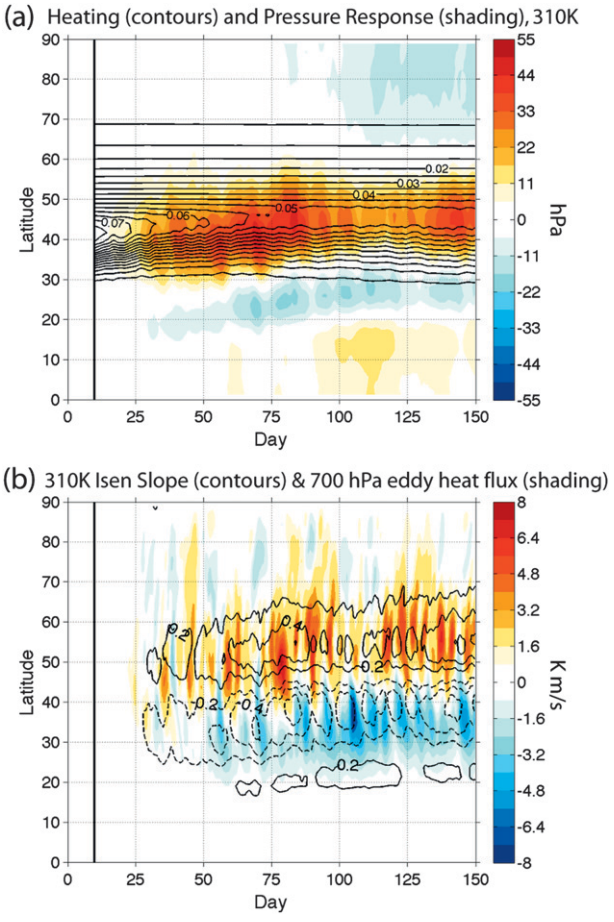

FIG. 4. (a) Contours indicate the projection of the thermal forcing onto the 310-K surface as a function of time and latitude. Contour interval is 0.005 K day^{-1}. Shading indicates the response of pressure at 310 K (hPa). (b) Contours indicate the response of the isentropic slope at 310 K. Contour interval is 0.2 m km^{-1} (meters in the vertical direction, kilometers in the meridional direction). The zero line is omitted. Positive values denote increasing height with latitude. Shading indicates the response of the eddy heat flux at 700 hPa (K m s^{-1}).

band spanned by the heating. The projection of the heating onto the 310-K surface changes as the isentropic surface moves with time and is most clearly aligned with the changes in pressure after about day 75.

The contours in Fig. 4b show the changes in the meridional slope of the 310-K surface (i.e., s_θ at 310 K) (m km^{-1}); the shading shows the response in the eddy heat fluxes at 700 hPa. As the 310-K isentrope moves to higher pressure around 40°–50° latitude (Fig. 4a), the meridional slope of the 310-K surface is reduced in the subtropics and increased in the extratropics (Fig. 4b). Thus, baroclinicity is decreased equatorward of about 40° but increased poleward of about 40°. The eddy fluxes of heat clearly respond in a manner consistent with forcing by the changes in the isentropic slope (Fig. 4b): regions where the meridional slope is increased are marked by anomalous poleward eddy fluxes of heat; regions where the meridional slope is decreased are marked by anomalous equatorward eddy fluxes of heat. As the integration proceeds, the eddy fluxes of heat will also adjust the slope of the isentropic surfaces. But the results in Fig. 4b strongly suggest that the eddy fluxes are to first order responding to the changes in baroclinicity driven by the tropical heating.

The results in Fig. 4 thus reveal two key aspects of the dynamical response to tropical heating: 1) the projection of the heating onto the initial isentropic surfaces determines the initial changes in the meridional slopes of the isentropic surfaces, and 2) the changes in the meridional slopes of the isentropes, in turn, lead to changes in the eddy fluxes of heat—that is, regions where the isentropic slopes are flattened (where the flow is stabilized) are marked by anomalously equatorward eddy fluxes of heat, and regions where the isentropic slopes are increased (where the flow is destabilized) are marked by anomalously poleward eddy fluxes of heat. The anomalous eddy fluxes of heat are thus downgradient in the sense that they are oriented away from the latitude of maximum heating. Similar results are found for isentropic surfaces between 300 and 320 K and for the eddy heat fluxes at pressure levels lower than 700 hPa (not shown). Surfaces below 300 K intersect the ground in the subtropics, making the results there more difficult to interpret.

b. Eddy fluxes of PV near the tropopause

The results in Fig. 4 suggest that two physical factors contribute to the lower tropospheric response to tropical heating: the effect of the tropical heating on the meridional slope of lower tropospheric isentropic surfaces and the diffusive nature of the eddy heat fluxes. As shown below, a diffusive model of the eddy fluxes also provides a close approximation for the changes in the eddy fluxes of PV near the tropopause.

Figures 5a and 5b show the distribution of PV (contours) and the eddy fluxes of PV (shading) averaged over days 100–150 for the (Fig. 5a) unforced and (Fig. 5b) forced experiments. In general, the eddy fluxes of PV are oriented along the axis of the dynamical tropopause (i.e., where PV $\approx$ 2 PVU) and peak near 60°. There is a secondary maximum in the eddy fluxes of PV in the midlatitude stratosphere, but the stratospheric response is not examined in this study. The primary differences between Figs. 5a and 5b lie near the subtropical tropopause, where the heating acts to noticeably decrease PV and lift both the dynamical tropopause and the region of largest eddy PV fluxes.

The differences between Figs. 5a and 5b are quantified in Fig. 5c. The contours show the differences in PV; the

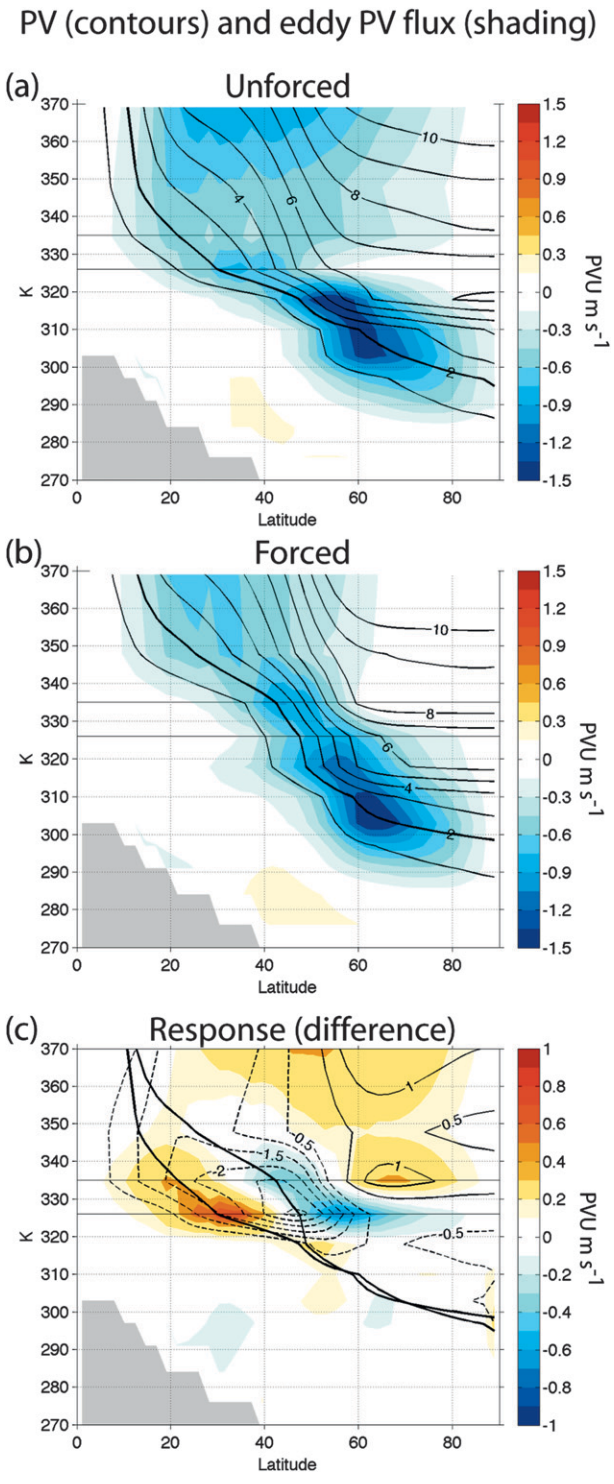

FIG. 5. PV (contours, PVU) and the eddy flux of PV (shading, PVU m s^{-1}) averaged over days 100–150 for (a) the unforced experiment, (b) the forced experiment, and (c) the response (i.e., the difference). The thin horizontal lines show 335- and 326-K isentropes. The solid black lines in (a) and (b) correspond to the 2-PVU contour; the solid black lines in (c) reproduce the 2-PVU contour from the unforced experiment (lower line) and forced experiment (upper line).

shading shows the changes in the eddy fluxes of PV. The thick solid lines show the 2-PVU contour for the unforced (lower line) and forced (upper line) experiments. As noted above, the heating leads to widespread decreases in PV near the subtropical tropopause centered around 40°–50°. The decreases in PV are driven primarily by changes in static stability (not shown) and correspond to a lifting of the dynamical tropopause. The anomalous eddy fluxes of PV are down the anomalous gradients in the PV field; that is, the fluxes are anomalously poleward in the vicinity of the tropopause between about 20° and 40° and anomalously equatorward between about 50° and 60°.

The pattern of anomalous eddy PV fluxes in Fig. 5c corresponds to the anomalous divergence of the EP flux in the subtropics and convergence of the EP flux in midlatitudes between about 320 and 340 K [(6)]. Thus, the results indicate a poleward shift in the latitude of largest wave breaking at those levels. Since the anomalous eddy fluxes of PV are down the anomalous gradients in PV, it follows that they do not drive the anomalous potential vorticity anomalies. Rather, the anomalous eddy PV fluxes can be interpreted as responding to the changes in the mean distribution of PV.

At first glance, the wave forcing of the tropopause-level zonal-wind anomalies may appear counterintuitive: the anomalous zonal flow is eastward in regions of anomalous equatorward PV fluxes (anomalous EP flux convergence), and vice versa. However, the anomalous upper-level PV fluxes are dominated not by the meridional convergence of the momentum flux (which determines the barotropic component of the response), but by the vertical derivative of the heat flux [second term on the rhs of (6); result not shown]. The anomalous vertical derivative of the heat flux gives rise to anomalous PV fluxes that act to damp the upper-level zonal wind anomalies, much as the climatological-mean equatorward PV fluxes act to damp the climatological-mean eastward flow near the extratropical tropopause (as is also true in the observations; e.g., Green 1970). The response of the upper tropospheric zonal flow should be viewed not in terms of the in situ wave forcing but rather as the sum of the barotropic component of the response (which is determined by the meridional convergence of the momentum flux) and the thermal wind. The barotropic component of the response is discussed further in section 5.

Figure 6 explores the evolution of the upper-level responses in PV (contours) and the eddy fluxes of PV (shading) as a function of latitude and time on two isentropic surfaces: 326 and 335 K. The surfaces are chosen because 1) they lie within the region of largest anomalous PV fluxes (Fig. 5c; light horizontal lines) and 2) they correspond to model levels. In the unforced

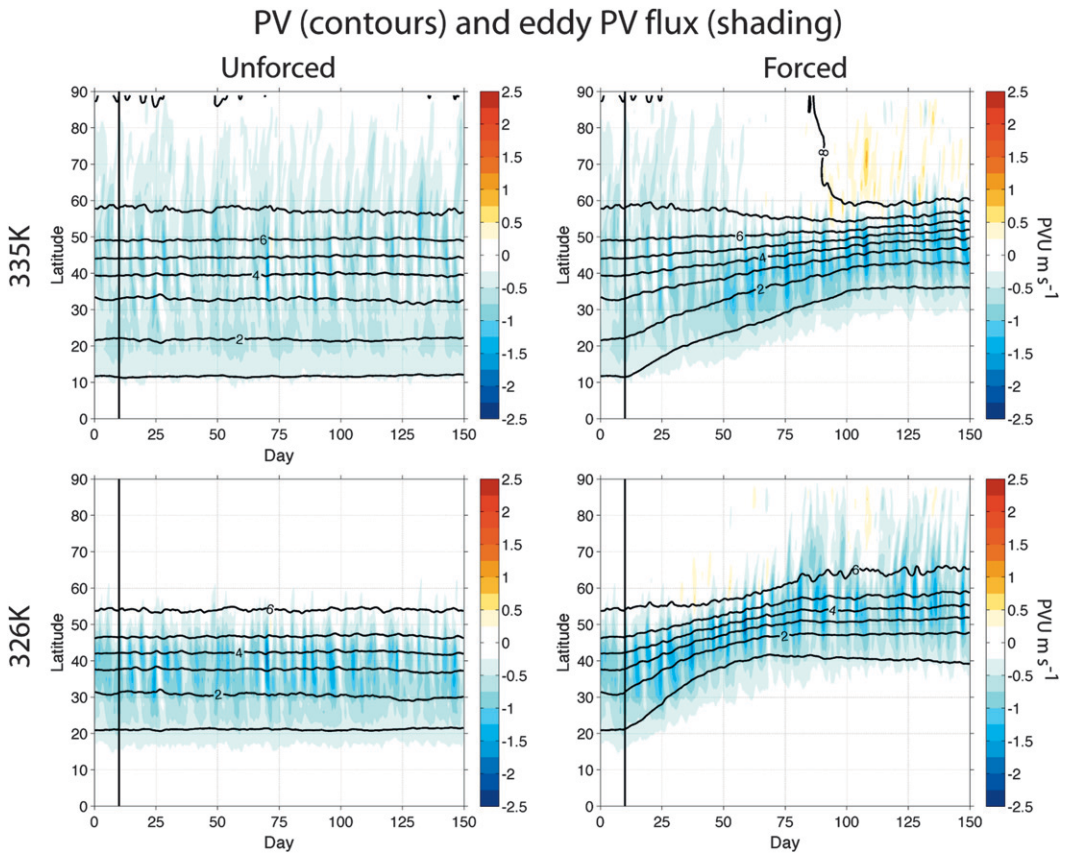

FIG. 6. PV (contours, PVU) and the eddy flux of PV (shading, PVU m s^{-1}) as a function of time and latitude at (top) 335 and (bottom) 326 K. Results are shown for the (left) unforced and (right) forced experiments.

experiment (Fig. 6, left panels), the gradients in PV are fairly uniform between 10° and 60° at 335 K but are concentrated over a relatively narrow latitude band at 326 K. In the forced experiment (Fig. 6, right panels), PV decreases in the subtropics immediately after the heating is turned on at day 10 (particularly at 326 K), and hence the regions of largest PV gradients are pushed toward the pole. By day 100, the regions of largest PV gradients are centered notably poleward of their original locations on both isentropic surfaces. At 335 K the region of largest PV gradients is not only pushed poleward but is also compressed meridionally. In both the unforced and forced experiments, the largest equatorward eddy fluxes of PV (blue shading) closely follow the gradients in the PV field (i.e., as the gradients in PV are pushed poleward by the heating, so are the attendant eddy fluxes of PV).

The poleward shift in the eddy fluxes of PV shown in Fig. 6 reflects a poleward shift in the latitude of largest wave drag in the vicinity of the subtropical tropopause. The eddy fluxes of PV evidently track the regions of largest PV gradients, and thus the response of the total wave driving near the tropopause seems consistent with a diffusive model of the eddy fluxes. That is, tropical heating changes the gradients in PV near the tropopause level through its effects on static stability; the eddy fluxes of PV adjust in a manner consistent with the flux–gradient relationship.

5. Summary and discussion

a. *Summary*

Tropical heating leads to a robust poleward contraction of the extratropical jets and their eddy fluxes of heat and PV in a range of numerical experiments. The experiments analyzed here reveal the following novel aspects of the eddy response to such heating in the dry dynamical core of a general circulation model:

1) In general, heating in the tropical troposphere directly affects the meridional slope of the isentropes in the subtropical and extratropical troposphere through its projection on the climatological-mean isentropic surfaces. In the specific case considered here, the heating intersects lower tropospheric isentropic surfaces not in the deep tropics but in the

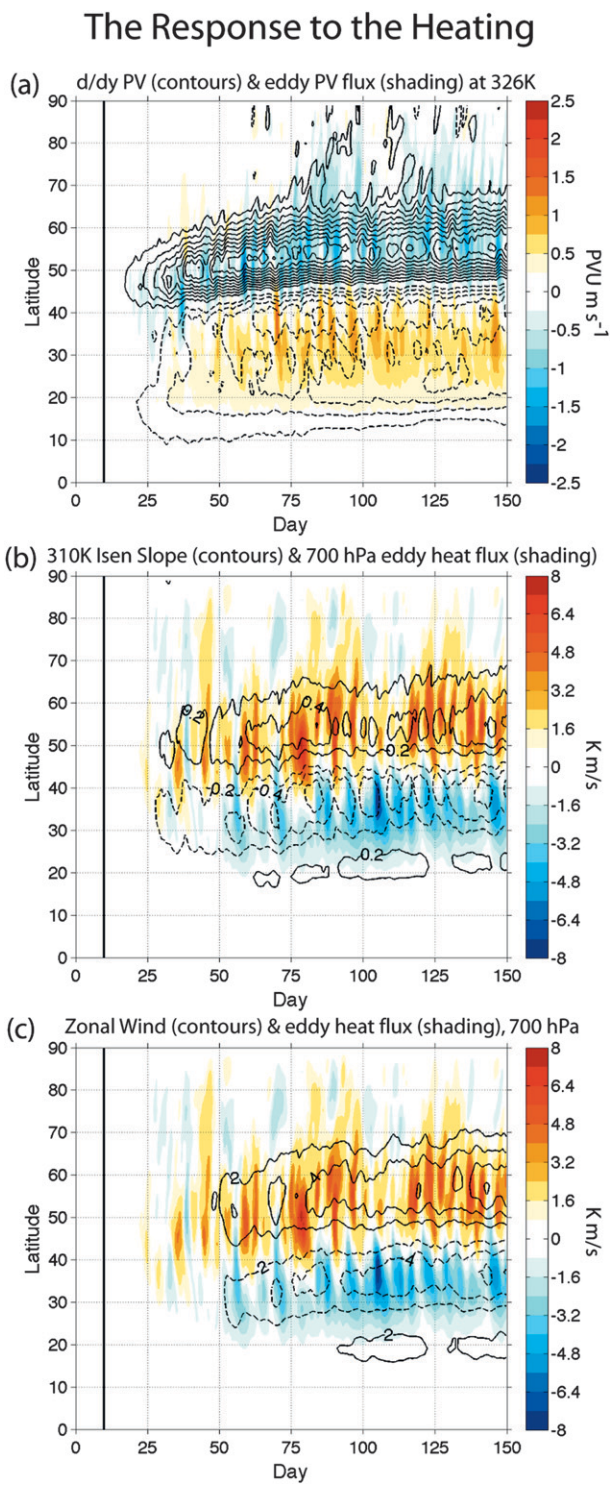

FIG. 7. The response to the heating as a function of time and latitude. (a) Contours indicate the meridional gradient in PV at 326 K. Contour interval is 0.25×10^{-12} PVU m^{-1}. Shading indicates the eddy PV flux at 326 K. (b) Reproduced from Fig. 4b. Contours indicate the response of the isentropic slope at 310 K. Positive values denote increasing height with latitude. Contour interval is 0.2 m km^{-1} (meters in the vertical direction, kilometers in the meridional direction). Shading indicates the response of the eddy heat flux at 700 hPa. (c) Contours indicate the response of the zonal wind at 700 hPa. Contour interval is 2 m s^{-1}. The zero line is omitted. Shading indicates the response of the eddy heat flux at 700 hPa. The unit of eddy PV fluxes is PVU m s^{-1}; the unit of eddy heat fluxes is K m s^{-1}.

subtropics. As such, the heating increases the isentropic slope in the extratropics and decreases the slope in the subtropics.

2) The changes in the isentropic slope are coincident with anomalous heat fluxes in the lower troposphere: the poleward eddy fluxes of heat are increased in regions where the isentropic slopes are anomalously steep and decreased where the isentropic slopes are flattened. Thus, the poleward shift in the latitude of lower tropospheric eddy heat fluxes is consistent with the direct effect of the heating on the baroclinic stability of the extratropical troposphere.
3) At upper levels, the heating leads to low PV in the vicinity of the subtropical tropopause via its effects on atmospheric static stability. The anomalous eddy fluxes of PV (which are indicative of the wave forcing near the tropopause) are down the gradient of the anomalies in the PV field. Thus, the poleward shift in wave breaking at the tropopause is consistent with a diffusive model of the eddy fluxes of PV: regions where the pole–equator gradients in PV are increased are marked by enhanced equatorward eddy fluxes of PV, and vice versa.

The key results of this study are summarized in Fig. 7. Figure 7a shows the response to the heating in terms of the gradients in the PV field (contours) and the eddy fluxes of PV (shading) at 326 K; Fig. 7b shows the response in terms of the isentropic slope at 310 K (contours) and the eddy fluxes of heat at 700 hPa (shading). The results in Fig. 7a are derived by taking the difference between the gradients of the results in Fig. 6b and 6c; the results in Fig. 7b are reproduced from Fig. 4b.

The anomalous eddy fluxes of PV (Fig. 7a) and heat (Fig. 7b) are both down the gradient of the anomalies in the zonal-mean circulation. At the tropopause, the decrease in PV is largest near 45° (Fig. 5c); thus, the anomalous equator–pole PV gradient at the tropopause is negative in the subtropics but positive at middle latitudes (Fig. 7a). The associated anomalous eddy fluxes of PV are downgradient in both regions (Fig. 7a). In the lower midtroposphere, the anomalous eddy fluxes of heat are downgradient in the sense that they are anomalously poleward where the baroclinicity is enhanced, and vice versa (Fig. 7b).

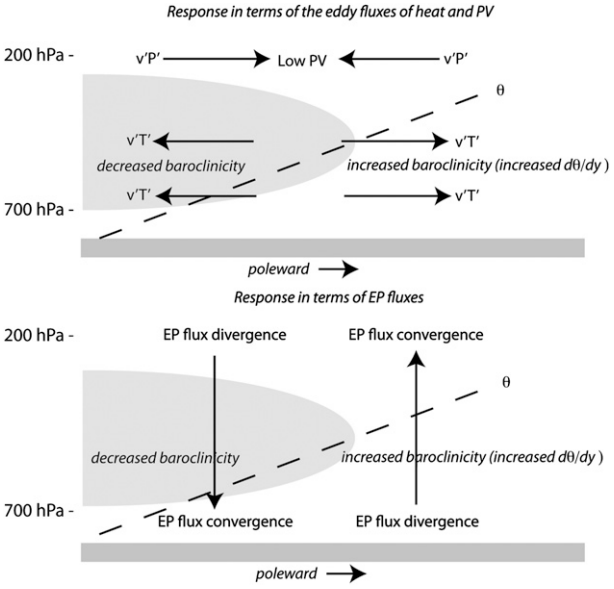

FIG. 8. Schematic of the response to tropical tropospheric heating (light gray shading) in terms of (top) the anomalous eddy fluxes of heat and PV and (bottom) the anomalous EP fluxes and their divergences. The heating intersects the isentropic surface (dashed line) in the subtropics. Thus, the heating increases (decreases) the isentropic slope (i.e., the baroclinicity) poleward (equatorward) of the region where the isentrope intersects the heating. At the same time, the reduction in static stability above the heating leads to low PV there. The heat fluxes are anomalously poleward where the baroclinicity is increased, and vice versa, whereas the anomalous PV fluxes are downgradient as indicated. The downgradient PV fluxes are consistent with a diffusive model of the eddy fluxes at the tropopause, as indicated in the top panel, but they are also mandated by the vertical derivative of the heat flux, which is indicated in terms of the anomalous EP flux in the bottom panel. See text for details.

The anomalous eddy fluxes of heat and PV shown in Figs. 7a and 7b exhibit a high degree of vertical coherence (i.e., regions of anomalous poleward heat fluxes near the surface are overlain by regions of anomalous equatorward PV fluxes at the tropopause, and vice versa). As noted in section 4, the strong degree of vertical coherence is consistent with the fact that the PV fluxes aloft are driven by the anomalous tropospheric heat fluxes as they damp at the tropopause level. Thus, the anomalous eddy fluxes of heat and PV in Figs. 7a and 7b do not arise independently. Rather, they are both a consequence of the changes in the heat fluxes within the free troposphere.

To indicate this more clearly, Fig. 8 shows a schematic representation of the results in this paper. The top panel shows the tropospheric response in terms of the eddy fluxes of heat and PV; the bottom panel shows the same response in terms of the anomalous EP fluxes and their divergences. The direct effect of the heating is to reduce PV at the tropopause (via a decrease in static stability), reduce the isentropic slope (reduce baroclinicity) in the subtropical troposphere, and increase the isentropic slope (increase baroclinicity) in the midlatitude troposphere. The eddy response includes anomalous poleward eddy heat fluxes where the baroclinicity is increased, anomalous equatorward heat fluxes where the baroclinicity is decreased, and anomalous downgradient eddy fluxes of PV at the tropopause.

When viewed solely from the perspective of the PV field at the tropopause, the anomalous eddy fluxes of PV can be interpreted as due to the in situ anomalous PV gradients (Fig. 8, top panel). However, when viewed from the perspective of the lower troposphere, the anomalous eddy fluxes of PV are clearly also due to the changes in tropospheric baroclinicity and thus the source of wave activity in the troposphere (Fig. 8, bottom panel). That is, the changes in eddy heat fluxes within the troposphere give rise to anomalous divergence of the vertical component of the EP flux in the vicinity of the subtropical tropopause, as well as anomalous convergence of the vertical component of the EP flux in the vicinity of the midlatitude tropopause. Presumably, both the source of wave activity within the troposphere and the gradients in PV at the tropopause play a role in determining the total changes in the eddy PV fluxes aloft.

b. Discussion

As noted in section 2, there are several caveats to the diffusive model when applied to the eddy fluxes of PV. Most importantly, radiation plays a first-order role in determining the surface gradients in temperature, but the eddies themselves play a first-order role in determining the PV gradients aloft (e.g., Held 1999). The key role of the eddies in setting the PV gradients in the free atmosphere complicates the interpretation of cause and effect between the eddies and the mean flow there. Additionally, the eddy flux of PV consists of two primary terms: the vertical gradient in the eddy heat flux and the horizontal gradient in the eddy momentum flux. Thus, anomalies in the eddy fluxes of PV are not necessarily indicative of changes in the barotropic component of the flow (i.e., the component driven by the vertically integrated eddy momentum flux convergence).

In principle, the results could be used to provide a precise quantitative estimate of the changes in the eddy fluxes if 1) we estimated the eddy diffusivities and 2) the eddy diffusivities are assumed to remain fixed in response to the heating. However, the eddy diffusivities are extremely noisy when calculated directly from data (they are proportional to the meridional PV flux divided by the spatial gradients in PV). Additionally, there is no a priori reason to expect the diffusivities to remain fixed in time. Nevertheless, a diffusive model of the eddy fluxes

of PV has been applied with apparent success toward problems such as the height of the tropopause (e.g., Schneider 2004), and the results shown here suggest that such a model provides an excellent qualitative approximation of the eddy response to diabatic heating at the tropopause level. The diffusive model also provides a qualitative approximation of the barotropic component of the flow (for reasons to be set forth below).

Theoretically, the eddy forcing that drives the barotropic component of the response can be quantified by vertically integrating the anomalous eddy fluxes of PV from the surface (where the PV flux is equivalent to the heat flux) to the top of the atmosphere. In practice, the barotropic component of the response can be estimated from the response in the lower tropospheric eddy heat flux. That is because the lower tropospheric eddy heat flux reflects the generation of wave activity near the surface. Assuming that a component of the wave activity generated near the surface propagates meridionally in the free atmosphere, it follows that latitude bands marked by anomalously poleward heat fluxes at the surface are accompanied by anomalous eddy momentum flux convergence aloft, and vice versa (e.g., Robinson 1996, 2000). Thus, regions of anomalous poleward heat fluxes should coincide with anomalous eastward flow at the surface, and regions of anomalous equatorward heat fluxes should coincide with anomalous westward flow at the surface. The meridional coincidence between eddy heat fluxes and the surface flow has been used to explain the persistence of annular variability (e.g., Robinson 1996, 2000) and was exploited recently by Lu et al. (2010) to explain the simulated surface wind response to changes in sea surface temperatures.

Figure 7c provides support for the above line of reasoning. The shading shows the response of the eddy heat fluxes at 700 hPa (reproduced from the middle panel); the contours show the response of the zonal wind at 700 hPa. There is evidently a high degree of correspondence between the changes in the near-surface flow and the near-surface heat fluxes: regions of anomalous poleward surface heat fluxes are accompanied by anomalous eastward wind anomalies and thus—by inference—anomalous convergence of the eddy momentum flux aloft; regions of anomalous equatorward surface heat fluxes are accompanied by anomalous westward wind anomalies.

The results in this study provide a mechanism for interpreting the tropospheric eddy response to diabatic heating other than that outlined in Chen and Held (2007) and Chen et al. (2008). Following the mechanism outlined in those studies, the response to tropical heating can be interpreted as follows: 1) the heating leads to eastward zonal wind anomalies at the extratropical tropopause via thermal wind, 2) the anomalies in the thermal wind lead to an increase in the eddy phase speed and thus drive a poleward shift in the latitude of largest wave breaking in the subtropics, and 3) the poleward shift in wave breaking in the subtropics induces a meridional circulation that perturbs baroclinicity and thus wave generation at lower levels. In contrast, the mechanism outlined here suggests that 1) the poleward shift in wave generation at lower levels is driven fundamentally by the projection of the heating onto the isentropic surfaces at extratropical latitudes, and 2) the poleward shift in wave breaking near the tropopause is due to the poleward shift in the heat fluxes within the troposphere (which converge at the tropopause level) and the diffusive nature of the eddy fluxes of PV. Which mechanism is most applicable to the real atmosphere remains to be determined.

We applied a heating profile that spans the entire tropical troposphere and decreases monotonically along pressure surfaces (Fig. 1). The heating projects onto the upward sloping isentropic surfaces at subtropical latitudes and thus leads to a dipole in baroclinicity, with increased baroclinicity in the extratropics and decreased baroclinicity in the subtropics. The changes in the eddy fluxes of heat and PV will also adjust the baroclinicity as the integration proceeds. But as shown in Fig. 4, the eddy response is to first order consistent with the changes in baroclinicity forced directly by the diabatic heating.

Presumably, the changes in extratropical baroclinicity should be very different for heatings that do not intersect the upward sloping isentropic surfaces in the subtropics. But interestingly, dipolar changes in baroclinicity very similar to those shown in Fig. 4 also arise for heatings that are confined to the deep tropics [i.e., as in Fig. 2c of Butler et al. (2010); results not shown]. The robustness of the dipole in baroclinicity to the meridional scale of the heating suggests that the weak horizontal temperature gradients in the tropical atmosphere (Charney 1963) place a strong constraint on the structure of the extratropical response: that is, tropical heatings with both narrow and broad meridional scales yield nearly identical patterns of tropical temperature rises (Butler et al. 2010; cf. their Fig. 2) and thus have very similar influences on the meridional slopes of the isentropic surfaces at subtropical latitudes. It is not immediately clear why the response to the warm phase of the El Niño–Southern Oscillation yields a seemingly opposite-signed response to that shown here (Chen et al. 2010), although the absence of moisture in our experiments may a play a key role in this regard. We considered damping the decreases in subtropical baroclinicity by applying a heating that decreases monotonically along isentropic

surfaces (i.e., rather than pressure surfaces). But in practice, the resulting heating profiles appear unphysical when projected onto pressure coordinates (e.g., consider a heating profile that follows the 310-K surface in Fig. 1a).

We have applied a (macro) turbulence perspective to the extratropical eddy response to imposed tropical heating. In our view, the extratropical response is—to first order—driven by dry dynamical processes. However, moist processes must inevitably play a key role in determining the true shape and amplitude of the tropical heating. It would be interesting to test the hypotheses outlined here in experiments forced not by idealized tropical heating, but by realistic changes in sea surface temperatures in a climate model that includes moist processes.

Acknowledgments. We thank R. Alan Plumb, Dennis Hartmann, Dargan Frierson, Ed Gerber, Gang Chen, Joe Kidston, and Michelle L'Heureux for helpful discussion of the results. We also thank Jian Lu, one anonymous reviewer, and the JAS editor for their insightful comments. Thanks to David Randall and Ross Heikes for use of the CSU AGCM and computing hours at NERSC. David W. J. Thompson is supported by the NSF Climate Dynamics Program. Amy H. Butler was supported by the EPA STAR Graduate Fellowship program and the NSF Climate Dynamics Program for the portion of this work completed at CSU.

REFERENCES

Arblaster, J., and G. Meehl, 2006: Contributions of external forcings to southern annular mode trends. *J. Climate,* **19,** 2896–2905.

Brayshaw, D. J., B. Hoskins, and M. Blackburn, 2008: The storm-track response to idealized SST perturbations in an aqua-planet GCM. *J. Atmos. Sci.,* **65,** 2842–2860.

Butler, A. H., D. W. J. Thompson, and R. Heikes, 2010: The steady-state atmospheric circulation response to climate change–like thermal forcings in a simple general circulation model. *J. Climate,* **23,** 3474–3496.

Charney, J. G., 1963: A note on large-scale motions in the tropics. *J. Atmos. Sci.,* **20,** 607–609.

Chen, G., and I. Held, 2007: Phase speed spectra and the recent poleward shift of Southern Hemisphere surface westerlies. *Geophys. Res. Lett.,* **34,** L21805, doi:10.1029/2007GL031200.

——, J. Lu, and D. M. W. Frierson, 2008: Phase speed spectra and the latitude of surface westerlies: Interannual variability and global warming trend. *J. Climate,* **21,** 5942–5959.

——, R. A. Plumb, and J. Lu, 2010: Sensitivities of zonal mean atmospheric circulation to SST warming in an aqua-planet model. *Geophys. Res. Lett.,* **37,** L12701, doi:10.1029/2010GL043473.

Chen, P., and W. A. Robinson, 1992: Propagation of planetary waves between the troposphere and stratosphere. *J. Atmos. Sci.,* **49,** 2533–2545.

Frierson, D. M. W., 2008: Midlatitude static stability in simple and comprehensive general circulation models. *J. Atmos. Sci.,* **65,** 1049–1062.

Fyfe, J., G. Boer, and G. Flato, 1999: The Arctic and Antarctic oscillations and their projected changes under global warming. *Geophys. Res. Lett.,* **26,** 1601–1604.

Green, J. S. A., 1970: Transfer properties of the large-scale eddies and the general circulation of the atmosphere. *Quart. J. Roy. Meteor. Soc.,* **96,** 157–185.

Hegerl, G. C., and Coauthors, 2007: Understanding and attributing climate change. *Climate Change 2007: The Physical Science Basis,* S. Solomon et al., Eds., Cambridge University Press, 663–745.

Heikes, R. P., and D. A. Randall, 1995: Numerical integration of the shallow water equations on a twisted icosahedral grid. Part I: Basic design and results of tests. *Mon. Wea. Rev.,* **123,** 1862–1880.

Held, I. M., 1999: The macroturbulence of the troposphere. *Tellus,* **51,** 59–70.

——, and M. J. Suarez, 1994: A proposal for the intercomparison of the dynamical cores of atmospheric general circulation models. *Bull. Amer. Meteor. Soc.,* **75,** 1825–1830.

——, and T. Schneider, 1999: The surface branch of the zonally averaged mass transport circulation in the troposphere. *J. Atmos. Sci.,* **56,** 1688–1697.

Kidston, J., G. K. Vallis, S. M. Dean, and J. A. Renwick, 2011: Can the increase in the eddy length scale under global warming cause the poleward shift of the jet streams? *J. Climate,* **24,** 3764–3780.

Konor, C., and A. Arakawa, 1997: Design of an atmospheric model based on a generalized vertical coordinate. *Mon. Wea. Rev.,* **125,** 1649–1673.

Kushner, P. J., and I. M. Held, 1998: A test, using atmospheric data, of a method for estimating oceanic eddy diffusivity. *Geophys. Res. Lett.,* **25,** 4213–4216.

——, ——, and T. L. Delworth, 2001: Southern Hemisphere atmospheric circulation response to global warming. *J. Climate,* **14,** 2238–2249.

Lim, E.-P., and I. Simmonds, 2008: Effect of tropospheric temperature change on the zonal mean circulation and SH winter extratropical cyclones. *Climate Dyn.,* **33,** 19–32, doi:10.1007/s00382-008-0444-0.

Lindzen, R. S., and B. F. Farrell, 1980: A simple approximate result for maximum growth rate of baroclinic instabilities. *J. Atmos. Sci.,* **37,** 1648–1654.

Lorenz, D. J., and E. T. DeWeaver, 2007: Tropopause height and zonal wind response to global warming in the IPCC scenario integrations. *J. Geophys. Res.,* **112,** D10119, doi:10.1029/2006JD008087.

Lu, J., G. Chen, and D. M. W. Frierson, 2008: Response of the zonal mean atmospheric circulation to El Niño versus global warming. *J. Climate,* **21,** 5835–5851.

——, ——, and ——, 2010: The position of the midlatitude storm track and eddy-driven westerlies in aquaplanet AGCMs. *J. Atmos. Sci.,* **67,** 3984–4000.

Matsuno, T., 1970: Vertical propagation of stationary planetary waves in the winter Northern Hemisphere. *J. Atmos. Sci.,* **27,** 871–883.

McIntyre, M. E., 2008: Potential-vorticity inversion and the wave-turbulence jigsaw: Some recent clarifications. *Adv. Geosci.,* **15,** 47–56.

Miller, R. L., G. A. Schmidt, and D. T. Shindell, 2006: Forced annular variations in the 20th century Intergovernmental Panel on Climate Change Fourth Assessment Report models. *J. Geophys. Res.,* **111,** D18101, doi:10.1029/2005JD006323.

Ringler, T. D., R. P. Heikes, and D. A. Randall, 2000: Modeling the atmospheric general circulation using a spherical geodesic grid: A new class of dynamical cores. *Mon. Wea. Rev.,* **128,** 2471–2490.

Robinson, W. A., 1996: Does eddy feedback sustain variability in the zonal index? *J. Atmos. Sci.,* **53,** 3556–3569.

——, 2000: A baroclinic mechanism for the eddy feedback on the zonal index. *J. Atmos. Sci.,* **57,** 415–422.

Schneider, T., 2004: The tropopause and the thermal stratification in the extratropics of a dry atmosphere. *J. Atmos. Sci.,* **61,** 1317–1340.

——, P. A. O'Gorman, and X. J. Levine, 2010: Water vapor and the dynamics of climate changes. *Rev. Geophys.,* **48,** RG3001, doi:10.1029/2009RG000302.

Tung, K. K., 1986: Nongeostrophic theory of zonally averaged circulation. Part I: Formulation. *J. Atmos. Sci.,* **43,** 2600–2618.

Williams, G. P., 2006: Circulation sensitivity to tropopause height. *J. Atmos. Sci.,* **63,** 1954–1961.

Yin, J. H., 2005: A consistent poleward shift of the storm tracks in simulations of 21st century climate. *Geophys. Res. Lett.,* **32,** L18701, doi:10.1029/2005GL023684.